

# Hardware MIMO Channel Simulator for Cooperative and Heterogeneous 5G Networks with VLC Signals

Bachir Habib<sup>(✉)</sup> and Badih Baz

Department of CS, Faculty of Sciences, USEK, Kaslik, Lebanon  
{bachirhabib, badihbaz}@usek.edu.lb

**Abstract.** This paper presents the design of an  $8 \times 8$  Multiple-Input Multiple-Output (MIMO) hardware simulator for cooperative time-varying propagation channels (based on relays) using heterogeneous systems (LTE-A and 802.11ac) with Visible Light Communications (VLC) signals. The simulator reproduces a desired radio channel scenario and makes it possible to test “on table” different systems. It uses different impulse responses to cover many types of channels by merging TGn models, 3GPP-LTE models, outdoor-to-indoor measurements results and VLC models. An algorithm is introduced to convert the measured impulse responses from 200 MHz sample frequency to 50 MHz to be compatible with LTE-A signals. A specific architecture of the simulator digital block is presented to characterize 5G scenarios. The architecture is designed on a Xilinx Virtex-VII XC7VX690T Field Programmable Gate Array (FPGA). Its accuracy and FPGA occupation are analyzed.

**Keywords:** Hardware simulator · FPGA · MIMO · Wireless heterogeneous systems · Cooperative networks

## 1 Introduction

MIMO techniques [1], cooperative networks and heterogeneous systems [2, 3] became essential in the design of the 5G communication systems. Moreover, VLC technologies [4–7] (LED or laser based), that are under development, show that they could be more than 100 times faster than current Wi-Fi. Therefore, all these technologies have to be considered in the design of any channel simulator platform that makes it possible to predict the received signal for any transmitted signal for a defined environment. With continuing increase of the FPGA capacity, entire baseband simulators can be mapped onto faster FPGAs for more efficient prototyping and testing [8–11].

Several architectures of the digital block of a hardware simulator have been studied [9, 12]. Typically, radio channels are simulated using Finite Impulse Response (FIR) filters [12, 13]. The Fast Fourier Transform (FFT) module with algebraic product can also be used. However, the FFT operates correctly only for signals not exceeding the FFT size. Thus, new frequency architecture avoiding this limitation has been presented and tested in [14]. However, it has been shown [15, 16] that the time domain architecture is better in terms of occupation on FPGA, output error and latency. Thus, in this paper, only the time domain architecture is considered.

Impulse responses must be implemented in the simulator to test a desired environment. They can be obtained from standard models, as the TGN 802.11n [17] (for indoor channels) and the LTE models [18] (for outdoor channels), or by using measurements conducted with a MIMO channel sounder realized at IETR [19] to cover outdoor-to-indoor channels. In MIMO context, little experimental results have been obtained regarding time-variations due to several limitations of the channel sounding equipment [19]. However, theoretical models of time-varying channels can be obtained using Rayleigh fading and Kronecker method [20, 21].

The main contributions of the paper are:

- An algorithm is presented to switch between several outdoor environments and make it possible to simulate heterogeneous radio propagation channels.
- An algorithm is used for the measured impulse responses to switch from 200 MHz sampling frequency ( $f_s$ ) to 50 MHz and make it compatible with LTE-A.
- Two new 5G scenarios are proposed. They consider heterogeneous networks that switch between WLAN and mobile networks. They also consider cooperative networks by using cell phones in the environment as relays.
- Simulation of 5G  $8 \times 8$  MIMO systems using VLC Li-Fi signals is considered.
- The new simulator architecture is implemented on a Virtex VII FPGA. It has better precision compared to [14–16] due to the use of 16 bits DAC/ADC.

The work structure with the contributions is shown in Fig. 1.

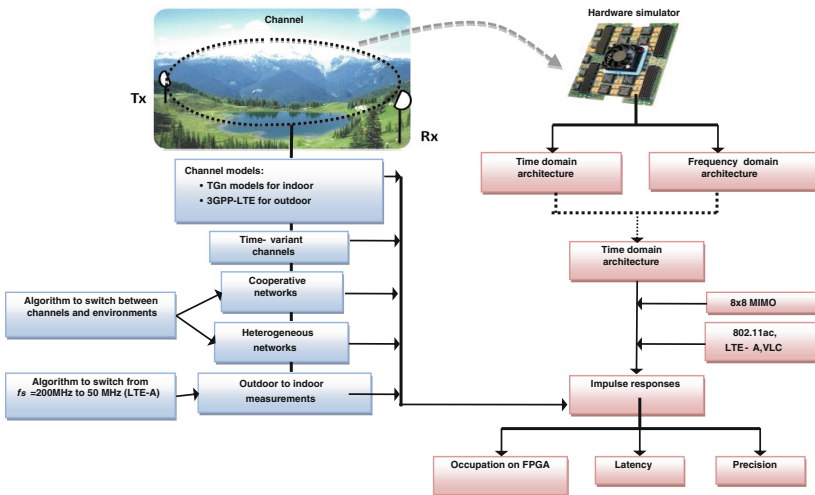


Fig. 1. Work structure. (Color figure online)

The rest of this paper is organized as follows. Section 2 presents the channel characteristics. Section 3 describes the architecture and its hardware implementation. In Sect. 4, the architecture accuracy is analyzed and results are presented. Lastly, Sect. 5 gives concluding remarks and prospects.

## 2 Channel Characteristics

### 2.1 Channel Description

Two scenarios are proposed to test the simulator architecture. They cover outdoor, outdoor-to-indoor and indoor environments at different environmental speeds. They consider the movements of a person from an environment to another using:

- LTE-A signal with a sampling frequency ( $f_s$ ) of 50 MHz, a sampling period ( $T_s$ ) of 20 ns, a bandwidth ( $B$ ) of 20 MHz and a central frequency ( $f_c$ ) of 1.8 GHz.
- 802.11ac signal with  $f_s = 165$  MHz,  $T_s = 6$  ns,  $B = 80$  MHz and  $f_c = 5$  GHz.
- VLC Li-Fi red laser signal for Line-Of-Sight (LOS) communication with a frequency of 472, 440 GHz. It is used especially between base stations.
- VLC Li-Fi red LED signal for LOS and Non-LOS (NLOS) communication with a frequency of 472, 440 GHz. It is used for indoor environments instead of Wi-Fi.

Figure 2 and Table 1 describe the two scenarios in details. In both scenarios, the person driving his vehicle moves from an urban environment to a highway. In this context, another base station is used as a relay. The signal transmitted between the 2 base stations (in LOS) is done using Li-Fi red laser to have fast communication and to surpass the frequency capacity spectrum. On the highway he exits the covered area by the base station. Therefore, the cooperative networks concept is used. Another person's cell phone between the transmitter (Tx) and the receiver (Rx) is used as a relay. It receives the signal, amplify it and retransmit it.

In the first scenario, the person (in red in Fig. 1) walks to his home. When he enters, he will receive an outdoor-to-indoor signal. Therefore, the channel will be simulated using measurements obtained by a campaign realized to retrieve outdoor-to-indoor impulse responses. Later, the system switches to LED Li-Fi once receiving a powerful signal using heterogeneous systems handover techniques [3].

In the second scenario, the person (in black in Fig. 1) switches to 802.11ac signal. This case is considered to simulate heterogeneous systems without VLC signals.

For LOS communications, as in the case of VLC Li-Fi red laser signal, the impulse responses are computed by using the relation  $d^{-\gamma}$  between the average received power and the distance to determine the attenuation of the signal, where  $\gamma$  is the path loss exponent and it is equal to 2. The delay of the signal is computed by considering the speed of light as a reference.

The models used are the LTE Extended Vehicular A (EVA), the LTE Extended Typical Urban (ETU), the LTE Extended Pedestrian A (EPA) [18] and the TGn model D, C and B [17].  $v$  is the mean environmental speed,  $f_{ref}$  is the refresh frequency between two successive MIMO profiles,  $t$  is the duration of movements in the considered environment,  $d$  is the traveled distance and  $N_p = t \times f_{ref}$  is the number of profiles in each environment.  $f_d$  is the Doppler frequency.  $f_{ref}$  is chosen greater than  $2f_d$  to respect the Nyquist-Shannon sampling theorem.

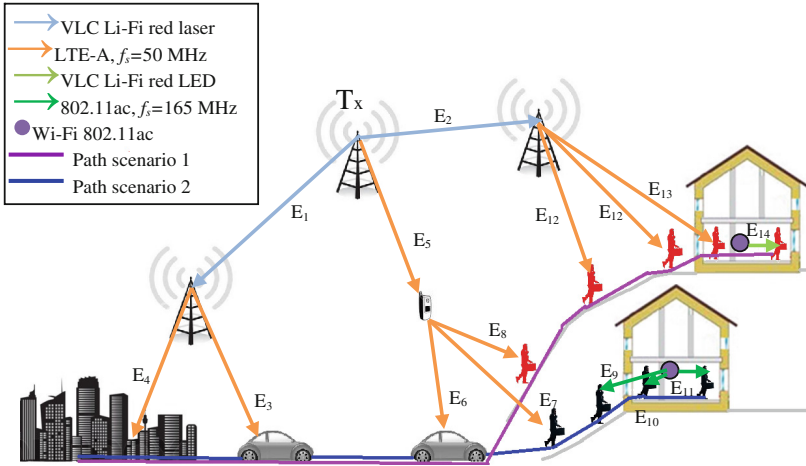


Fig. 2. Proposed scenarios. (Color figure online)

Table 1. Scenarios description.

Scenario/Env.	Model	v (km/h)	$f_c$ (GHz)	$f_d$ (Hz)	$f_{ref}$ (Hz)	t (s)	d (km)	$N_p$
1/E <sub>1</sub> E <sub>3</sub>	Li-Fi laser*ETU	0; 40	472T; 1.8	0; 66	0; 150	600	6.6	90,001
1/E <sub>1</sub> E <sub>4</sub>	Li-Fi laser*EVA	0; 80	472T; 1.8	0; 133	0; 275	600	13.3	165,001
1/E <sub>5</sub> E <sub>6</sub>	EPA*EVA	4; 80	1.8; 1.8	18.3; 133	40; 75	300	6.6	94,500
1/E <sub>5</sub> E <sub>8</sub>	EPA*EPA	4; 4	1.8; 1.8	18.3; 18.3	40; 40	180	0.2	14,400
1/E <sub>2</sub> E <sub>12</sub>	Li-Fi laser*EPA	0; 4	472T; 1.8	0; 18.3	0; 40	180	0.2	7,201
1/E <sub>2</sub> E <sub>13</sub>	Li-Fi laser*measures	0; 2	472T; 1.8	0; 9.1	0; 20	60	0.03	1,201
1/E <sub>14</sub>	Li-Fi LED	1.4	472T	6.5	15	30	0.01	450
2/E <sub>1</sub> E <sub>3</sub>	Li-Fi laser*ETU	0; 40	472T; 1.8	0; 66	0; 150	600	6.6	90,001
2/E <sub>1</sub> E <sub>4</sub>	Li-Fi laser*EVA	0; 80	472T; 1.8	0; 133	0; 275	600	13.3	165,001
2/E <sub>5</sub> E <sub>6</sub>	EPA*EVA	4; 80	1.8; 1.8	18.3; 133	40; 275	300	6.6	94,500
2/E <sub>5</sub> E <sub>7</sub>	EPA*EPA	4; 4	1.8; 1.8	18.3; 18.3	40; 40	180	0.2	14,400
2/E <sub>9</sub>	TGn D	4	5	18.3	40	180	0.2	7,200
2/E <sub>10</sub>	TGn C	2	5	9.1	20	60	0.03	1,200
2/E <sub>11</sub>	TGn B	1.4	5	6.5	15	30	0.01	450

## 2.2 Update Measurements to LTE-A and Environment Switch Algorithms

The measurements, using the MIMO channel sounder, were made with  $f_s = 200$  MHz. To use these measurements with LTE-A signals, many steps have to be done. To pass from baseband complex impulse responses to real impulse responses between  $[\Delta, B + \Delta]$ , the following formula is used where  $f_c = \Delta + B/2$ :

$$h(t) = h_p(t) \cos(2\pi f_c t) - h_q(t) \sin(2\pi f_c t) \quad (1)$$

The obtained real impulse responses must be limited between 0 and  $-20$  dB to select its significant part. Moreover, to decrease the number of non-null taps of the impulse responses, an algorithm is used which consists of detecting the taps considered as points of change for the sign of the slope of the curve.

Finally, to pass from  $f_s = 200$  MHz to 50 MHz, an algorithm is proposed. It consists on replacing each 4 successive taps ( $i, i + 1, i + 2, i + 3$ ), which have a sampling period  $T_s = 5$  ns ( $f_s = 200$  MHz), by one tap placed at  $i + 1$ . Thus, a new sampling period  $T_s = 20$  ns ( $f_s = 50$  MHz) is obtained. This new tap placed at  $i + 1$  is the sum of the linear Relative Powers (RP) of the 4 taps. A normalization algorithm is preceded on the RP to increase the simulator output signals precision. The results are obtained for  $8 \times 8$  MIMO system. Figure 3 presents the real impulse response on  $2048T_s$ , the impulse response used by the simulator after discrimination, normalization and limitation between  $[0, -20$  dB] of the measured impulse responses with  $f_s = 200$  MHz and the impulse responses compatible with LTE-A with  $f_s = 50$  MHz, for  $h_{11}$ . Moreover, the number of multipliers also decreases. In fact, it is divided by 4 due to the transition from  $f_s = 200$  MHz to  $f_s = 50$  MHz.

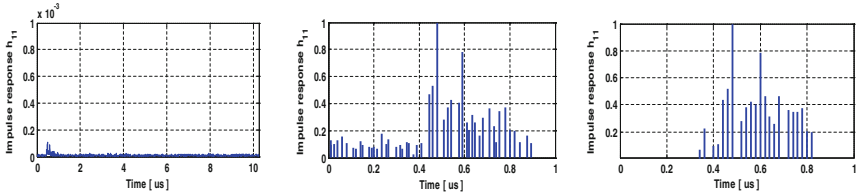


Fig. 3. Data Measured (left), used with  $f_s = 200$  MHz (middle), used with  $f_s = 50$  MHz (right).

The switch between the environments must be made in continuous mode. Between  $E_{10}$  and  $E_{11}$  for example, the person speed decelerate from 2 (km/h) to 1.4 (km/h). To pass from the  $RP$  of the last tap  $h_{ij}$  in  $E_{10}$  ( $RP_l$ ) to the first  $h_{ij}$  tap in  $E_{11}$  ( $RP_f$ ), a relation is proposed that varies the  $RP$  for each  $f_{ref}$ .  $f_{ref}$  also changes as in Table 1. It passes from 20 ( $f_{ref_1}$ ) to 15 Hz ( $f_{ref_f}$ ). The relations are:

$$RP_i = RP_l + (i - 1) \frac{RP_f - RP_l}{N - 1}, f_{ref_i} = f_{ref_1} + (i - 1) \times \frac{f_{ref_f} - f_{ref_1}}{N - 1} \quad (2)$$

where  $i$  is an integer that varies from 1 to  $N \cdot N = 80$ , in fact,  $80/((20 + 15)/2) = 4.5$  s is the needed time to switch between the impulse responses which is sufficient to pass from  $v = 2$  km/h ( $E_{I0}$ ) to  $v = 1.4$  km/h ( $E_{I1}$ ). Figure 4 presents the result of the 80 impulse responses ( $h$ ) while switching between channels.

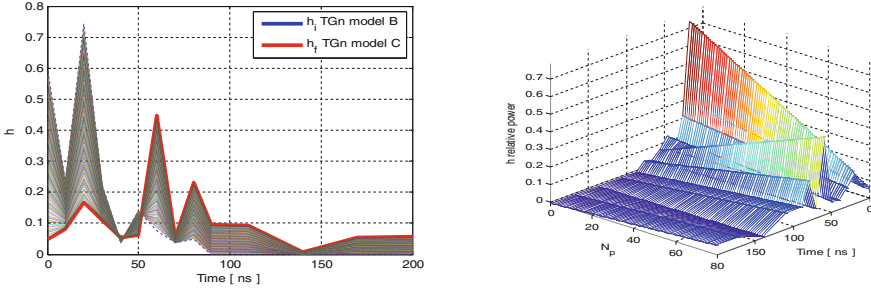


Fig. 4. Switching between TGn model B to TGn model C.

### 2.3 Channel Real Time Variation Using Rayleigh and Kronecker Method

After computing the impulse responses, this sub-section presents a method to vary the channel. The Rayleigh fading is used of each SISO channel. For  $2 \times 2$  MIMO fading channel, Kronecker method [21] is considered. It can be characterized by the relative power  $P_c$  (resp.  $P_s$ ) of constant (resp. scattering) channel components corresponding to LOS (resp. NLOS) paths. The ratio  $P_c/P_s$  is the Rice K-factor. The same concept is applied to  $8 \times 8$  MIMO. Assuming that all the elements of the MIMO channel matrix  $H$  are Rice distributed, it can be expressed for each tap by:

$$H = \sqrt{P_c} \cdot H_F + \sqrt{P_s} \cdot H_V \text{ with } P_c = P \cdot \frac{K}{K+1}, P_s = P \cdot \frac{1}{K+1} \quad (3)$$

where  $H_F$  and  $H_V$  are the constant and the scattered matrices respectively. The total received power is  $P = P_c + P_s$ ,  $K = 0$  to obtain Rayleigh fading. For 2 Tx/Rx:

$$H = \sqrt{P} \cdot \begin{bmatrix} X_{11} & X_{12} \\ X_{21} & X_{22} \end{bmatrix} \quad (4)$$

To correlate the  $X_{ij}$  elements, a product-based model is used. This model assumes that the correlation coefficients are independently derived at each end of the link:

$$X = (R_r)^{1/2} \cdot H_{iid} \cdot ((R_t)^{1/2})^T \text{ where } R_t = \begin{bmatrix} 1 & \alpha \\ \alpha^* & 1 \end{bmatrix}, R_r = \begin{bmatrix} 1 & \beta \\ \beta^* & 1 \end{bmatrix} \quad (5)$$

$H_{iid}$  is a matrix of independent zero means, unit variance, complex Gaussian random variables.  $R_t$  and  $R_r$  are the Tx/Rx correlation matrices. The correlation coefficients  $\alpha/\beta$  are expressed by  $\rho = R_{xx}(D) + j \cdot R_{xy}(D)$ ,  $D = 2\pi d/\lambda$ ,  $d = 0.5\lambda$  the distance between antennas with wavelength  $\lambda$ . The Power Angular Spectrum (PAS) matches the Laplacian distribution with  $\sigma$  the standard deviation. Thus:

$$\begin{aligned}
 R_{xx}(D) &= \int_{-\pi}^{\pi} \cos(D \cdot \sin(\varphi)) \cdot PAS(\varphi) \cdot d\varphi, R_{xy}(D) \\
 &= \int_{-\pi}^{\pi} \sin(D \cdot \sin(\varphi)) \cdot PAS(\varphi) \cdot d\varphi
 \end{aligned}
 \tag{6}$$

### 3 Digital Block Design of the Hardware Simulator

As the development board has 8 Analog-to-Digital Converter ADC (FMC168) and 8 Digital-to-Analog Converter DAC (FMC216), it will be connected to 8 down-conversion and 8 up-conversion RF units. 64 FIR filters are considered to simulate the  $8 \times 8$  MIMO channel. However, as the scenarios contain one relay (intermediate base station or cell phone), the number of FIR filters will be  $64 \cdot 2 = 128$  (Fig. 5).

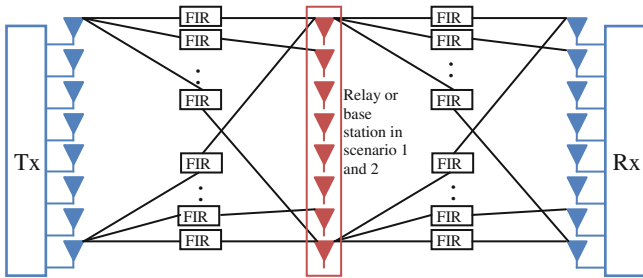


Fig. 5.  $8 \times 8$  MIMO system with relay.

The FIR width and the multipliers number are determined by the taps of each SISO channel. In a scenario, the entire SISO channels have to be considered. To use the limited number of multipliers of the FPGA, a solution is proposed to control the change of delays by connecting each multiplier to the corresponding cells of the shift register and RAM. Thus, the number of multipliers in the FIR filters is equal to the maximum number of taps of all SISO channels. 128 FIR filters, each one with 24 multipliers are considered. Figure 6 presents a FIR filter 250 with 24 multipliers for one SISO channel. We have developed our own FIR filter instead of using Xilinx filter to make it possible to reload the filter coefficients.

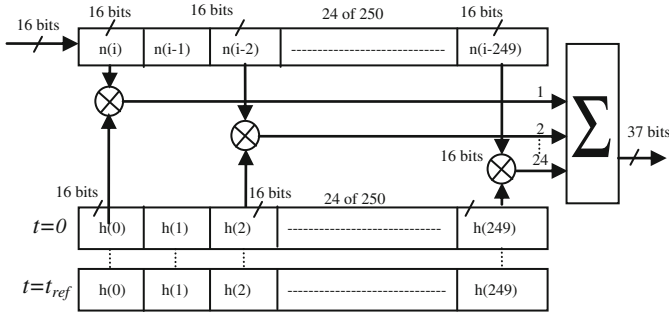


Fig. 6. FIR 250 with 24 multipliers for one SISO channel using  $h_{11}$ .

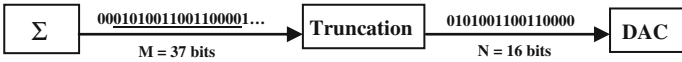



Fig. 7. Sliding window truncation, from 37 to 16 bits.

Due to the use of a 16-bit DAC, the final output must be truncated. The best solution is the sliding window truncation presented in Fig. 7 which uses the 16 most significant bits. The number of bits at the output before the truncation is:

$$n_y = n_h + n_x + n_{MIMO} + n_T \text{ where } n_{MIMO} = \lceil \log_2 N_T \rceil, n_T = \lceil \log_2 N_T \rceil \quad (7)$$

where  $n_y$  is the number of bits at the output before truncation,  $n_h$  is the number of bits at the impulse response, which is equal to 16 bits,  $n_x = 16$  is the number of bits of the input signal and  $N_T$  is the number of non-null taps of impulse responses.

Figure 8 shows the Xilinx Virtex-VII XC7VX690T [8] used for the implementation of the architecture. The simulations are made with ISE [8] and ModelSim [22]. It also shows the device utilization for 128 FIR filters of 24 multipliers each.



Logic Utilization	Used	Available	Utilization
Logic cells	199,351	693,120	29 %
Occupied Slices	98,457	108,300	91 %
RAM 18Kb blocks	11	2,940	1 %
DSP 25*18	3,072	3,600	86 %

Fig. 8. Virtex-VII FPGA board from Xilinx and FPGA occupation for 128 FIR filters.

The number of DSP multipliers is equal to:  $24 \text{ taps} * 128 \text{ FIR filters} = 3072$ . The impulse responses profiles are saved in the RAM memory blocks. The total number of profiles in the scenarios is 745,506. Each profile contains 128 channels each with 24 taps. For each tap the delay in time and the signal power must be known. Therefore, the total number of taps is:  $745,506 * 128 * 24 * 2 = 4,580,388,864$  taps of 16 bits each = 73,286,221,824 total bits. The capacity of each RAM block is 18 Kb. Thus, the number of blocks needed is:  $73,286,221,824 / 18 \text{ K} = 4,071,457$ .



However, the total number of RAM blocks on the FPGA is 2,940. Therefore, another method is used to save the impulse responses. They are saved on the computer and refreshed each  $f_{ref}$ . In this way, only 2 profiles are needed to be saved in the RAM blocks of the FPGA. In this case, the total number of taps is:  $2 \cdot 128 \cdot 24 \cdot 2 = 12,288$  taps of 16 bits = 196608 total bits = 11 RAM blocks < 2,940.

For a MIMO profile,  $24 \times 128 = 3072$  words of 16 bits = 6144 bytes have to be transmitted. Thus, the transfer speed is  $6144 \times f_{ref}$  Bps.

## 4 Results and Analysis

An input Gaussian signal  $x(t)$  is considered for all inputs. To obtain a signal that respects the bandwidth,  $x(t)$  centered between  $[\Delta, \Delta + B]$  is obtained by:

$$x(t) = x_m e^{-\frac{(t-m_x)^2}{2\sigma_x^2}}, \quad 0 \leq t \leq Wt, \quad \Rightarrow x(t) \rightarrow x(t) \cdot \cos\left(2\pi \cdot \left(\frac{B}{2} + \Delta\right) \cdot t\right) \quad (8)$$

In this work,  $\sigma_x = 3/\pi B$  is considered.  $m_x$  is chosen equal to  $20T_s > 3$  for both 802.11ac and LTE-A signals. Moreover,  $\Delta \ll B$  is chosen equal to 2 MHz. The ADC and DAC converters of the development board have a full scale  $[-V_m, V_m]$ , with  $V_m = 1$  V. For the simulations,  $x_m = V_m/2$  is considered.

The first theoretic output signals  $y_l(t)$  of the  $8 \times 8$  MIMO channel is computed by:

$$y_1(t) = h_{E_2 11}(t) * r_1(t) + h_{E_2 21}(t) * r_2(t) + \dots + h_{E_2 81}(t) * r_8(t) \quad (9)$$

where

$$r_u(t) = h_{E_1 1u}(t) * x_1(t) + h_{E_1 2u}(t) * x_2(t) + \dots + h_{E_1 8u}(t) * x_8(t) = \sum_{a=1}^8 h_{E_1 au}(t) * x_a(t) \quad (10)$$

Thus

$$y_k(t) = \sum_{b=1}^8 h_{E_2 bk}(t) * \sum_{a=1}^8 h_{E_1 ab}(t) * x_a(t) \text{ with } x * h = \sum_{k=1}^{Nt} h(i_k) \cdot x(t - i_k T_s) \quad (11)$$

The formula of the theoretical  $y_k(t)$  becomes:

$$y_k(t) = \sum_{b=1}^8 \sum_{q=1}^{Nq} \left( h_{E_2 bk}(i_q) \cdot \sum_{a=1}^8 \sum_{p=1}^{Np} \left( h_{E_1 ab}(i_p) \cdot x_a(t - (i_q + i_p)T_s) \right) \right) \quad (12)$$

where  $N_p$  and  $N_q$  are the number of taps of the impulse response and  $h(i_n)$  is the RP of the  $n^{th}$  path with the delay  $i_n T_s$ .

In order to determine the accuracy, a comparison is made between the theoretical/Xilinx output signals. Figure 9 presents a snapshot of the Xilinx output signal using Brutal (BT) and Sliding (ST) Truncations, with the theoretical signal, the relative error and the SNR for  $y_i(t)$  using measured outdoor-to-indoor data (left) and 3GPP-LTE model ETU (right) with and  $x_{LTE}(t)$  at the input. Figure 10 presents a snapshot of the result for  $y_i(t)$  using TGN model B (left) with  $x_{WLAN}(t)$  and VLC LED Li-Fi (right).

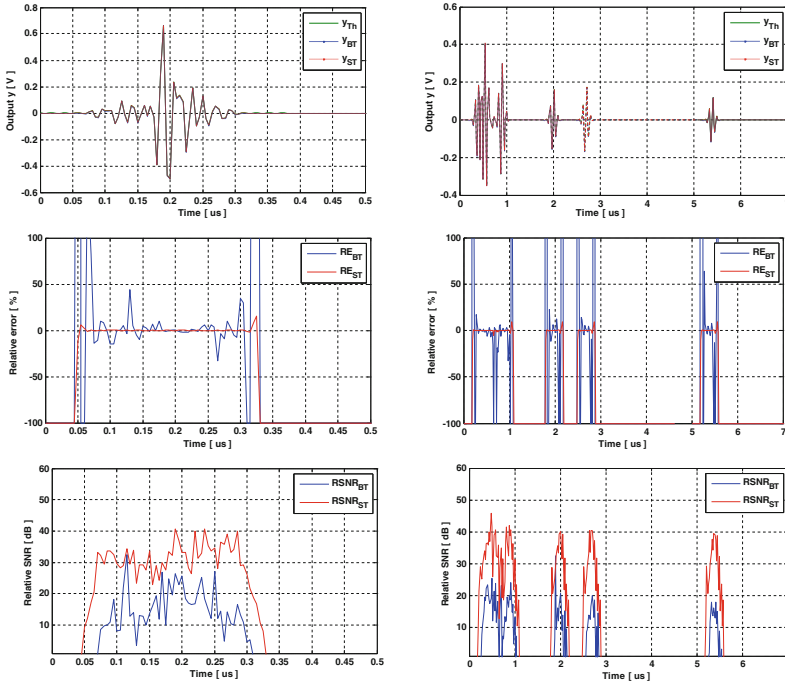


**Fig. 9.** Snapshot results for  $y_i$  using measured outdoor-to-indoor data (left) and 3GPP-LTE model ETU (right).

The relative error and SNR are computed by:

$$RE_k(i) = \frac{y_{qk}(i) - y_k(i)}{y_k(i)} \times 100, SNR_k(i) = 20 \log_{10} \left| \frac{y_k(i)}{y_{qk}(i) - y_k(i)} \right| [dB] \quad (13)$$

where  $y_{qk}$  is the vectors containing the samples of the Xilinx output signals.

The global relative error and global SNR are computed by:

$$RE_{Gk} = \frac{\|y_{qk} - y_k\|}{\|y_k\|} \times 100, SNR_{Gk} = 20 \log_{10} \frac{\|y_k\|}{\|y_{qk} - y_k\|} [dB] \quad (14)$$

Figure 11 presents the Global SNR variation in time for all profiles of  $y_1(t)$  and  $y_2(t)$  of four different environments of the scenarios. For the ETU environment only 1,000 profiles of 90,000 are presented.

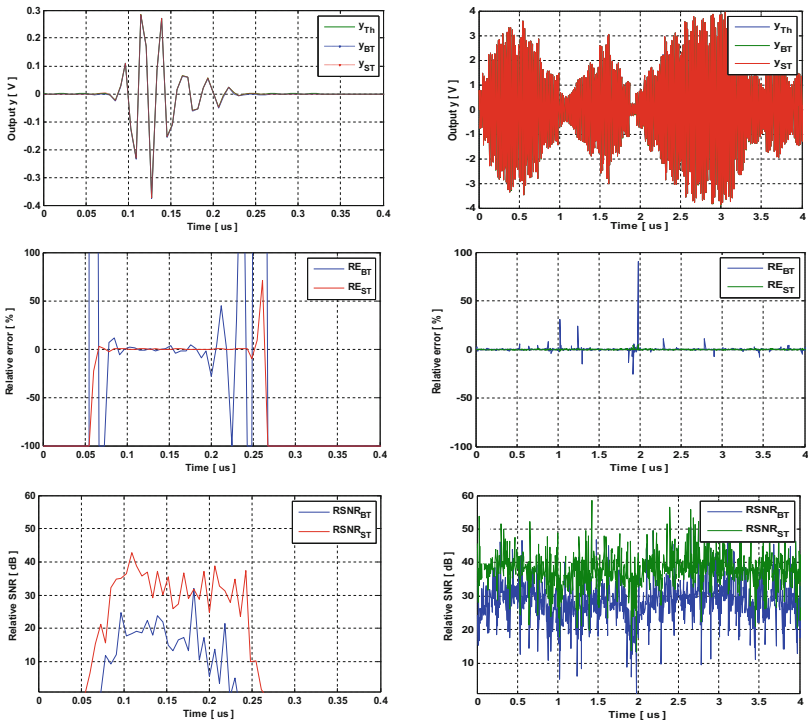


Fig. 10. Snapshot results for  $y_l$  using Tgn model B (left) and VLC LED Li-Fi (right).

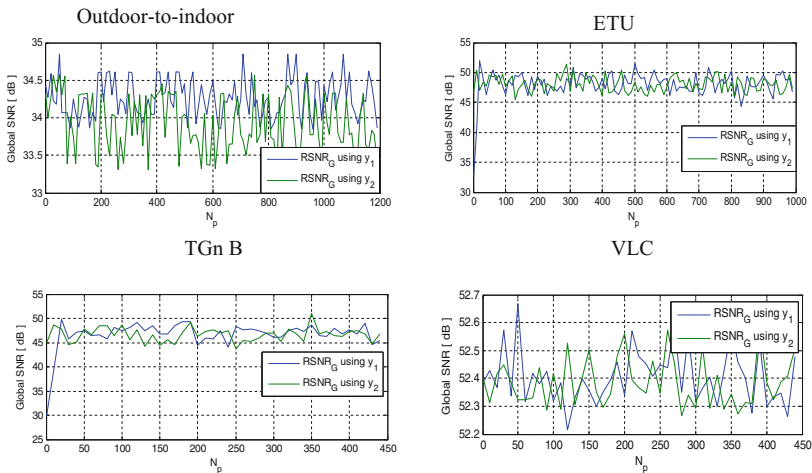


Fig. 11. Global SNR variation in time for  $y_1$  and  $y_2$ .

Table 2 shows the average total global SNR for different environments. The results are given with BT and ST.

**Table 2.** Global SNR (dB) for different environments of the scenarios.

	Outdoor-to-indoor	ETU	TGn model B	VLC LED
BT	34.32	49.15	47.12	52.38
ST	61.77	72.68	73.38	75.31

The table shows the benefit of a ST in the case of using real input signals that respects the band  $[\Delta, \Delta + B]$ . The previous figures of the relative errors show that the ST provides low variations (around zero %) for the relative error where the output signal is high. However, the BT presents high variations.

## 5 Conclusion

In this paper, tests have been made for scenario models that switch between different environments to simulate heterogeneous propagation environments and cooperative networks. Moreover, VLC signals are used. An algorithm has been proposed to switch between the environments in a continuous manner and another algorithm is introduced to convert the measured impulse responses from 200 MHz sample frequency to 50 MHz to be compatible with LTE-A signals. In order to simulate a time-varying channel, Rayleigh fading method is used to vary the relative power of the taps of the channel impulse response. The architecture of the  $8 \times 8$  MIMO simulator has been implemented on FPGA Virtex VII and analyzed.

This work can be completed by developing RF cards for the new standards and for heterogeneous systems. The hardware simulator realized considers the variation of the channel on small scale. Thus, variation on large scale must be considered. For the future cooperative communication systems, the Tx/Rx are in motion, the V2V concept has to be considered. Finally, the Tx/Rx distance has to be considered and simulation must be made not just for scenario models but also for real scenarios.

## References

1. Behbahani, S., Merched, R., El tawil, A.: Optimizations of a MIMO relay network. *IEEE Trans. Sig. Process.* **56**(10), 5062–5073 (2008)
2. Agyapong, P.K., Iwamura, M., Staehle, D., Kiess, W., Benjebbour, A.: Design Considerations for a 5G Network Architecture. *IEEE Commun Mag.* **52**, 65–75 (2014)
3. LTE Advanced: Heterogeneous Networks. Qualcomm Incorporated, January 2011
4. Cossu, G., Khalid, A.M., Choudhury, P., Corsini, R., Presi, M., Ciaramella, E.: VLC-signals distribution over GI-POF for in-home wireless networks. In: International Workshop on Optical Wireless Communications (IWOW), 22 October 2012, pp. 1–3 (2012)

5. Kim, Y., Shin, Y., Yoo, M.: VLC-TDOA using sinusoidal pilot signal. In: International Conference on IT Convergence and Security (ICITCS), 16–18 December 2013, pp. 1–3 (2013)
6. Yu, Z., Redfern, A.J., Zhou, G.T.: Using delta-sigma modulators in visible light OFDM systems. In: IEEE Wireless and Optical Communication Conference (WOCC 2014), May 2014, Newark, NJ (2014)
7. Arnon, S.: Visible Light Communication. Cambridge University Press, Cambridge (2015)
8. Xilinx: FPGA, CPLD and EPP solutions. [www.xilinx.com](http://www.xilinx.com)
9. Murphy, P., Lou, F., Sabharwal, A., Frantz, P.: An FPGA based rapid prototyping platform for MIMO systems. In: Asilomar Conference on Signals, Systems and Computers, ACSSC, 9–12 November 2003, vol. 1, pp. 900–904 (2003)
10. Wireless Channel Emulator. Spirent Communications (2006)
11. Baseband Fading Simulator ABFS: Reduced costs through baseband simulation. Rohde & Schwarz (1999)
12. Fouladi Fard, S., Ali Mohammad, A., Cockburn, B., Schlegel, C.: A single FPGA filter-based multipath fading emulator. In: Globecom, Honolulu, November 2009 (2009)
13. Eslami, H., Tran, S.V., Eltawil, A.M.: Design and implementation of a scalable channel emulator for wideband MIMO systems. *IEEE Trans. Veh. Technol.* **58**(9), 4698–4708 (2009)
14. Habib, B., Zaharia, G., El Zein, G.: MIMO hardware simulator: new digital block design in frequency domain for streaming signals. *J. Wirel. Netw. Commun.* **2**(4), 55–65 (2012)
15. Habib, B., Zaharia, G., El Zein, G.: MIMO hardware simulator: digital block design for 802.11ac applications with TGN channel model test. In: IEEE VTC Spring, Yokohama, Japan, May 2012 (2012)
16. Habib, B., Zaharia, G., El Zein, G.: Digital block design of MIMO hardware simulator for LTE applications. In: ICC, Ottawa, Canada (2012)
17. Erceg, V., Shumacher, L., Kyritsi, P., et al.: TGN channel models. In: IEEE 802.11-03/940r4, 10 May 2004
18. Agilent Technologies: Advanced design system – LTE channel model - R4-070872 3GPP TR 36.803 v0.3.0 (2008)
19. Farhat, H., Cosquer, R., Grunfelder, G., Le Coq, L., El Zein, G.: A dual band MIMO channel sounder at 2.2 and 3.5 GHz. In: IMTC, Victoria, BC, Canada, May 2008 (2008)
20. Almers, P., Bonek, E., et al.: Survey of channel and radio propagation models for wireless MIMO systems. *EURASIP J. Wirel. Commun. Netw.* **2007**, 1–19 (2007). Article ID 19070
21. Schumacher, L., Pedersen, K.I., Mogensen, P.E.: From antenna spacing to theoretical capacities – guidelines for simulating MIMO systems. In: PIMRC Conference, September 2002, vol. 2, pp. 587–592 (2002)
22. ModelSim - Advanced Simulation and Debugging. <http://model.com>